Journal of Power Sources 196 (2011) 10258–10262

Contents lists available at SciVerse ScienceDirect

Journal of Power Sources

journal homepage: www.elsevier.com/locate/jpowsour

Short communication

Morphology regulation and carbon coating of $LiMnPO_4$ cathode material for enhanced electrochemical performance

Fei Wang, Jun Yang*, Pengfei Gao, Yanna NuLi, Jiulin Wang

School of Chemistry and Chemical Engineering, Shanghai Jiao Tong University, 800 Dongchuan Road, Shanghai 200240, China

ARTICLE INFO

Article history:
Received 14 June 2011
Accepted 22 August 2011
Available online 27 August 2011

Keywords:
Lithium manganese phosphate
Solvothermal method
Nanoplate
Nanorod
Lithium-ion battery

ABSTRACT

Olivine-structured $LiMnPO_4$ with uniform cluster-like and rod-like morphologies have been synthesized via a simple solvothermal process in water–organic solvent mixtures. The cluster-like $LiMnPO_4$ microstructures are composed of numerous nanoplates in thickness of ca. 35 nm and width of ca. 400 nm. Carbon is coated on the $LiMnPO_4$ surfaces by chemical vapor deposition (CVD) from methylbenzene and ball milling with acetylene black, respectively. The hierarchical $LiMnPO_4$ nanoplates deliver much higher discharge capacity and rate capability than the nanorods due to the larger interfacial area for electrochemical reaction and shorter lithium ion diffusion depth. Furthermore, carbon-coating via CVD approach leads to a significant improvement in the electrochemical performances compared to the ball milling process.

1. Introduction

Olivine-type $LiMPO_4$ (M = Fe, Mn, Co and Ni) cathode materials have recently attracted much attention for lithium-ion batteries due to their low cost, large energy density, particularly high thermal and electrochemical stabilities [1–4]. Among these phosphates, $LiCoPO_4$ and $LiNiPO_4$ with very high voltage plateaus close to 4.8 V and 5.2 V are still difficult to be used in conventional electrolytes [5–7]. On the other hand, $LiMnPO_4$ provides a moderate working voltage compatible to the present electrolyte systems and can provide a higher energy density than $LiFePO_4$ on account of its higher redox potential of Mn^{3+}/Mn^{2+} (4.1 V) than Fe^{3+}/Fe^{2+} (3.5 V) [8]. However, the electric conductivity of $LiMnPO_4$ ($<10^{-10}$ S cm^{-1}) is extremely low, leading to a poor electrochemical activity [9,10]. In similar to $LiFePO_4$ material, many efforts have been made to improve the low intrinsic electronic and ionic conductivity of $LiMnPO_4$ by particle-size minimization, carbon coating and Mn-site doping [11–14].

Of different material synthesis technologies, the solvothermal process is an effective method to prepare nanostructured materials with well-defined morphology [15,16]. Murugan et al. [17] reported the nano-thumblike $LiMnPO_4$ with a diameter of ca. 60 nm by a microwave-solvothermal approach, showing a discharge capacity of 45 mAh g^{-1} at C/10. Saravanan et al. [18] synthesized $LiMnPO_4$ nanoplates via solvothermal method, which exhibited the largest discharge capacity of 52 mAh g^{-1} at C/10. Wang et al. [19,20] prepared $LiMnPO_4$ microspheres and nanorods by solvothermal process in ethanol–water mixed solvent, which delivered the discharge capacity of 107 and 127 mAh g^{-1} at C/100, respectively. Furthermore, the $LiMnPO_4$ nanoplates and nanorods were also successfully prepared by a polyol method and showed a discharge capacity as high as 145 mAh g^{-1} at C/20 and 120 mAh g^{-1} at 1 C, respectively [21,22].

In this paper, we describe a facile solvothermal synthesis method of $LiMnPO_4$ nanoplates and nanorods in a mixed solvent containing water and organic solvent (benzyl alcohol or polyethylene glycol). The effects of the material structure and carbon coating mode on the electrochemical performances are investigated and compared.

2. Experimental

2.1. Sample synthesis

Cluster-like $LiMnPO_4$ microstructures composed of numerous nanoplates were prepared as follows: a stoichiometric amount of $LiOH{\cdot}H_2O$, $MnSO_4{\cdot}H_2O$, H_3PO_4 and sodium dodecyl benzene sulfonate (SDBS) (mole ratio is 3:1:1:0.5) were added into water–benzyl alcohol mixed solvent (1:1, v/v). The concentration of Mn^{2+} in the precursors was 0.2 mol L^{-1}. After vigorous stirring, the suspension was transferred into a Teflon-lined stainless steel autoclave, followed by solvothermal treatment at 160 °C for 10 h. The product was filtered, washed and finally dried at 70 °C. For the synthesis of $LiMnPO_4$ nanorods, the same procedures were adopted

* Corresponding author. Tel.: +86 21 5474 7667; fax: +86 21 5474 7667.
E-mail address: yangj723@sjtu.edu.cn (J. Yang).

0378-7753/$ – see front matter © 2011 Elsevier B.V. All rights reserved.
doi:10.1016/j.jpowsour.2011.08.090

except that the mixed solvent was replaced by water–polyethylene glycol 400 (PEG400) mixture (1:1, v/v) without adding SDBS.

To increase the electronic conductivity of pristine $LiMnPO_4$, a carbon layer was coated by a CVD method using methylbenzene as carbon source and argon as carrier gas with a flow rate of 0.5 L min^{-1}. The CVD process was conducted at 800 °C for 20 min. The resulting $LiMnPO_4$/C composites are denoted as Plate-CVD and Rod-CVD. For a comparison, the bare $LiMnPO_4$ samples were carbon-coated by ball milling at 300 rpm for 6 h using 10 mm diameter zirconia balls. In the planetary mill (Pulverisette 6, Fritsch), the mass ratio of ball to powder was 15:1 and the powder contained 80% $LiMnPO_4$ and 20 wt% acetylene black. The obtained samples are denoted as Plate-BM and Rod-BM.

2.2. Sample analysis

The phase structure was characterized by X-ray diffraction (XRD) under a Rigaku D/Max-2200 diffractometer using Cu Kα radiation. The morphology and microstructure were observed by JEOL JSM-7401F field emission scanning electron microscope (FE-SEM) and transmission electron microscopy (TEM, JEOL JEM-2100). The amount of carbon was determined from PE 2400 II elemental analyzer. Brunauer–Emmett–Teller (BET) surface area was measured with a Micromeritics Instruments ASAP 2010 after the samples were vacuum dried at 200 °C for 4 h.

2.3. Electrochemical measurements

Electrochemical measurements were performed with CR2016 coin-type cells with lithium metal as anode. The cathodes were prepared by mixing 75 wt% active material, 15 wt% Super P carbon black and 10 wt% polyvinylidene difluoride (PVDF). Ethylene carbonate/dimethyl carbonate (EC:DMC = 1:1, v/v) mixed solution containing 1 M $LiPF_6$ was used as the electrolyte. Galvanostatic charge/discharge was controlled between 2.4 and 4.9 V at 25 °C on a Land CT2001 battery test system. Electrochemical impedance spectroscopic measurement (EIS) was conducted on a Solartron SI 1287 electrochemical interface in the frequency rang of 100 kHz to 0.01 Hz. To determine the extent of Mn dissolution into the electrolyte, the cells were disassembled after 20 cycles at 0.2 C rate, and the separator film plus cathode sheets were steeped in DMC solvent for 24 h. Finally, the amount of dissolved Mn in the electrolyte was detected by inductive coupled plasma emission spectroscopy (ICP, iCAP 6000 Radial).

3. Results and discussion

3.1. Sample characterization

Fig. 1 shows the SEM images of the samples. Cluster-like $LiMnPO_4$ hierarchical microstructures in the size of about 5–8 μm (Fig. 1a) are obtained from water–benzyl alcohol binary solvent. As shown in Fig. 1b, this microstructure is constructed by large numbers of uniform nanoplates in a size of ca. 35 nm in thickness and ca. 400 nm in width. It is notable that the preparation of the uniform nanoplates is highly dependent on both organic solvent and surfactant. The irregular plates and particles appeared without using the surfactant SDBS, while only aggregative particles were obtainable from pure water solvent (not shown here). By contrast, the $LiMnPO_4$ sample synthesized in water–PEG400 mixture has a rod-like shape with a diameter of 90–130 nm and a length up to 600 nm (Fig. 1c and d). Therefore, the organic solvent and the surfactant play

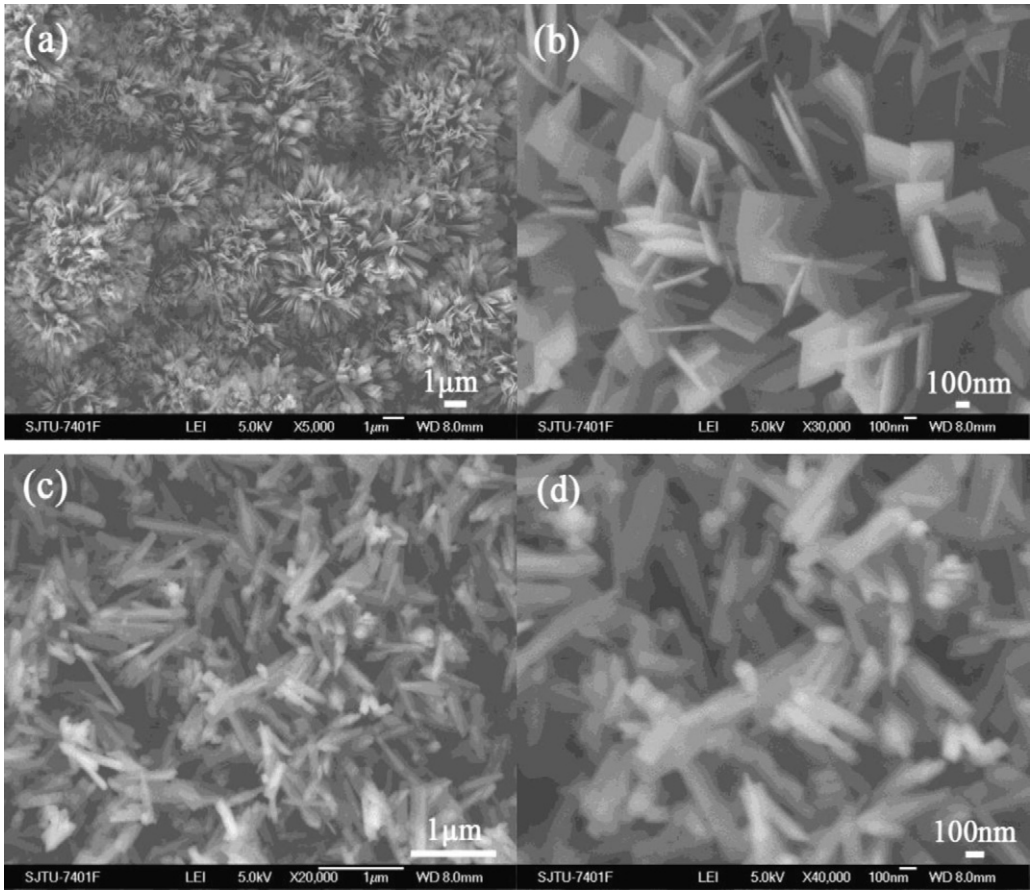

Fig. 1. SEM images of the $LiMnPO_4$ samples obtained from water–benzyl alcohol (a and b) and water–PEG400 (c and d) mixed solvent.

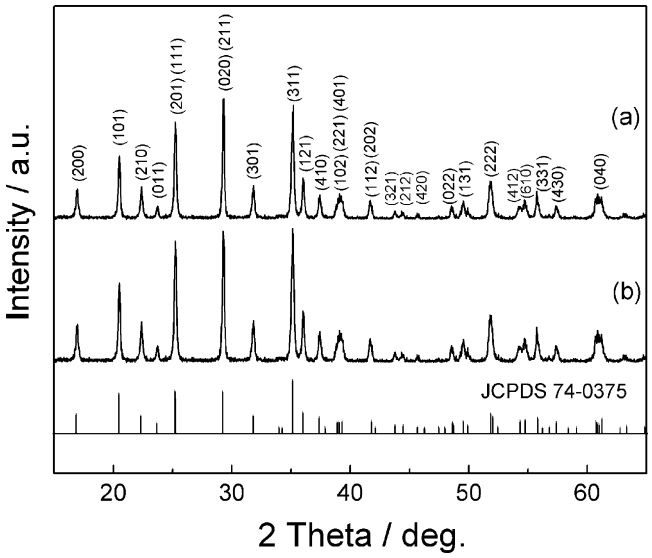

Fig. 2. XRD patterns of the $LiMnPO_4$ samples: nanoplates (a) and nanorods (b).

a crucial role in the morphology regulation during the solvothermal process. According to the nitrogen adsorption isotherm, the determined BET areas for cluster-like and rod-like $LiMnPO_4$ samples are 23.5 and 8.8 $m^2\ g^{-1}$, respectively.

The XRD patterns of $LiMnPO_4$ nanoplates and nanorods are shown in Fig. 2. Both the samples are well crystallized in orthorhombic olivine structure with a *Pnmb* space group. All the diffraction peeks are in good agreement with the standard $LiMnPO_4$ (JCPDS No. 74-0375). It is notable that the (0 2 0) peak intensity is the strongest for the cluster-like $LiMnPO_4$ nanoplates (Fig. 2a). As for the $LiMnPO_4$ nanorods (Fig. 2b), the peak intensity of (0 2 0) plane is almost the same as (3 1 1) plane. However, in the standard spectrum, the highest peak is related to the (3 1 1) plane. This suggests that these particles have a preferential crystal orientation along the (0 2 0) direction [21,23]. The refined lattice parameters of the $LiMnPO_4$ samples are $a = 10.4401$ Å, $b = 6.0881$ Å, and $c = 4.7422$ Å for the nanoplates and $a = 10.4446$ Å, $b = 6.1055$ Å, and $c = 4.7400$ Å for the nanorods, respectively. These values are consistent well with the literature data [12,20].

The TEM images of carbon-coated $LiMnPO_4$ nanoplate and nanorod by a CVD method and ball milling are presented in Fig. 3. After the CVD process, a fairly homogeneous carbon layer with a thickness in ca. 3 nm is covered tightly on the surface of $LiMnPO_4$ nanoplate in comparison with ca. 8 nm for $LiMnPO_4$ nanorod (Fig. 3a and b). Depending on elemental analysis, the carbon content in $LiMnPO_4$/C nanoplates and nanorods are about 8 wt% and 11 wt%, respectively. However, ball milling of $LiMnPO_4$ and acetylene black leads to an incomplete and loose carbon coverage on $LiMnPO_4$ (Fig. 3c and d).

Fig. 4 shows the TEM image and selected area electron diffraction (SAED) pattern of the $LiMnPO_4$ nanoplate. The SAED pattern in Fig. 4b is similar to the reported [0 1 0] SAED pattern of $LiMnPO_4$ and $LiFePO_4$ [17,18]. The c^*/a^* ratio in the reciprocal lattice is 2.20 from the SAED, accordant with the a/c ratio of lattice parameters for the $LiMnPO_4$ nanoplate with $a = 10.4401$ Å and $c = 4.7422$ Å. It reveals that the large plate face is in the *ac* plane (Fig. 4a) and the *b* direction is just the thinnest direction of the nanoplate. This result agrees well with the XRD data. As it has been proved that lithium ion preferably diffuses along the *b* axis in the $LiMPO_4$ orthorhombic olivine structure during the charge–discharge process [24,25], this thin plate morphology is favorable for rapid ionic diffusion to achieve high rate performance.

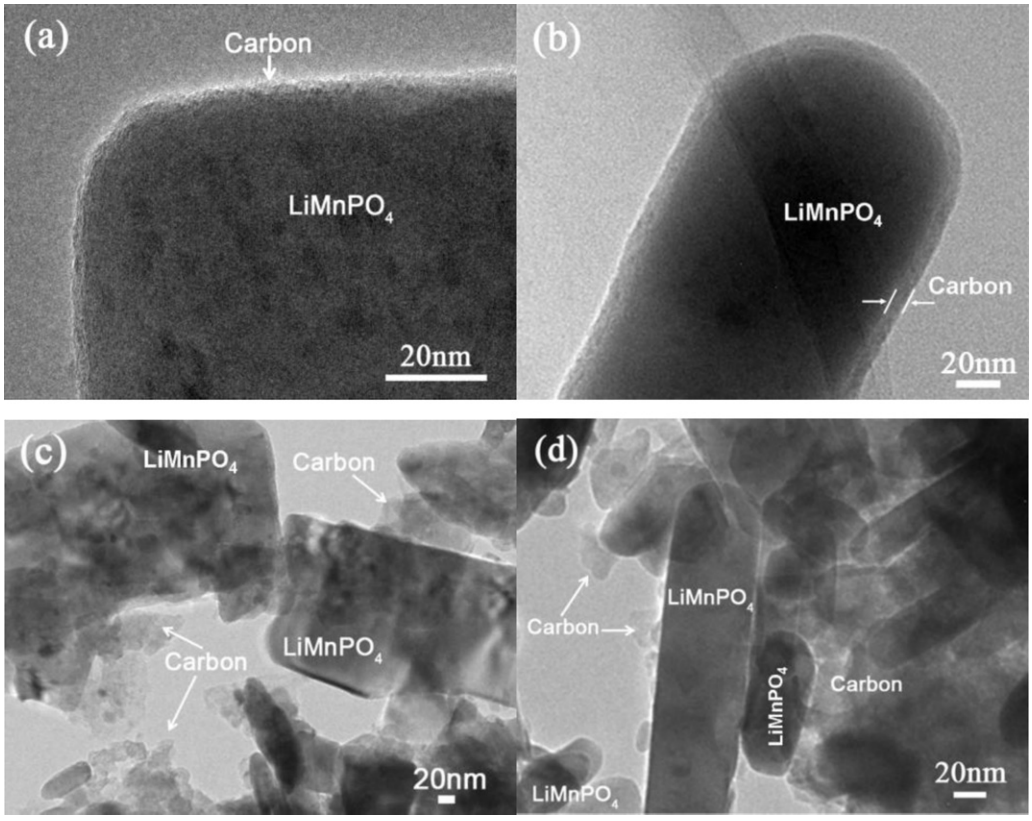

Fig. 3. TEM images of the $LiMnPO_4$ carbon-coated by a CVD process: nanoplate (a), nanorod (b); by ball milling: nanoplate (c), nanorod (d).

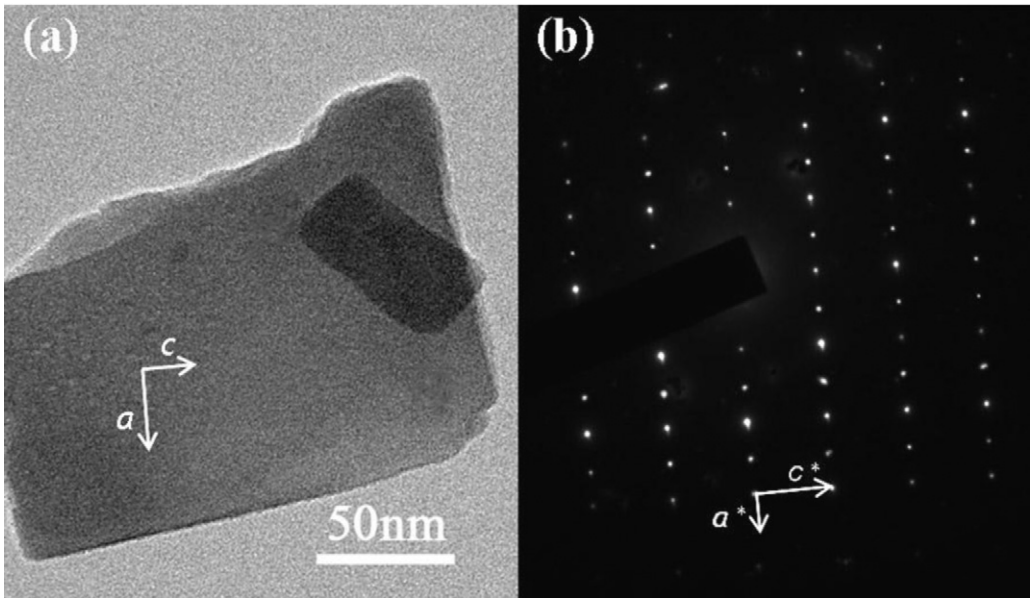

Fig. 4. TEM image of the $LiMnPO_4$ nanoplate (a) and the corresponding SAED pattern (b).

3.2. Electrochemical properties

Fig. 5 shows the typical (second) charge and discharge profiles of the different $LiMnPO_4$/C electrodes with a current rate of 0.05 C (8.5 mAh g^{-1}). All the electrodes present a reversible voltage plateau around 4.1 V, corresponding to the redox couple of Mn^{3+}/Mn^{2+}. The discharge capacities of Plate-CVD, Rod-CVD, Plate-BM and Rod-BM are 147, 126, 120 and 92 mAh g^{-1}, respectively. The $LiMnPO_4$ carbon-coated by CVD method delivers a significantly larger discharge capacity than that by ball milling. Moreover, the $LiMnPO_4$/C nanoplates exhibit superior electrochemical activity to the nanorods. This result indicates that both the morphology and carbon coating mode greatly influence the available capacity of $LiMnPO_4$.

Fig. 6 gives a comparison of the cyclic stability of four $LiMnPO_4$/C electrodes. The specific capacity of Plate-CVD sample decreases from 147 to 137 mAh g^{-1} up to 50 cycles and 93% of the initial capacity can be retained at 0.05 C rate. For Rod-CVD, Its capacity retention is also up to 90% in spite of a distinctly lower cycle capacity. On the other hand, the capacity retention is only 85% for Plate-BM and 81% for Rod-BM. The Mn dissolution in the electrolyte could be an important reason for capacity decrease of $LiMnPO_4$ [13]. The amounts of dissolved Mn in the electrolyte after 20 cycles at 0.2 C are 1.3, 1.0, 13.9, and 9.6 ppm for Plate-CVD, Rod-CVD, Plate-BM and Rod-BM, respectively. This indicates that the CVD method is more effective than ball milling to reduce Mn dissolution into the electrolyte. The bare $LiMnPO_4$ samples can be encapsulated completely with a carbon layer via the CVD process, which avoids the direct electrode/electrolyte contact and protects the $LiMnPO_4$ electrode against HF erosion during long-term cycling. Unfortunately, the ball milling method can only bring $LiMnPO_4$ material with a partial carbon coating, which leads to more side reactions at the electrode/electrolyte interface and poor cyclic performance.

Fig. 7 illustrates the discharge rate capability of $LiMnPO_4$/C nanoplates and nanorods ranging from 0.1 C to 5 C. For all the test cells, the charge rate remains constant at 0.1 C to insure identical initial conditions for each discharge. The Plate-CVD sample performs better than the Rod-CVD thoroughly. The capacity retention of nanoplates at 2 C is 67% compared with the capacity at 0.1 C. Nevertheless, this value is only 30% for nanorods. In addition, its

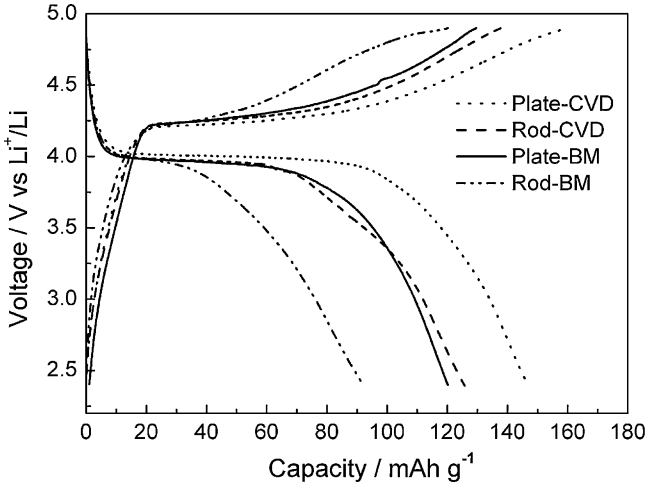

Fig. 5. The second charge/discharge profiles of the $LiMnPO_4$/C electrodes at 0.05 C rate.

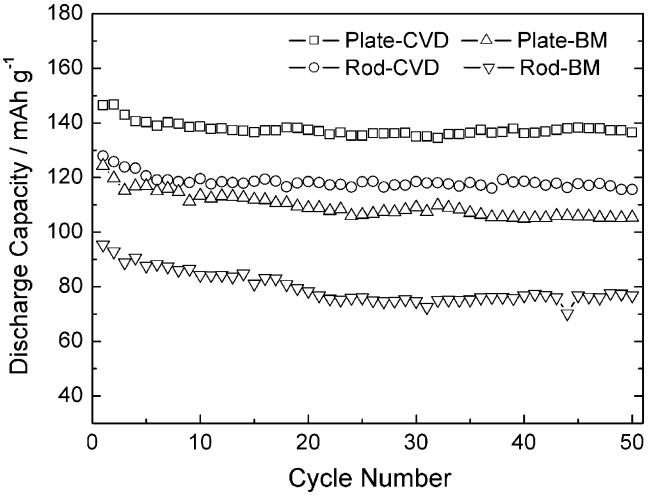

Fig. 6. Cycling performances of the $LiMnPO_4$/C electrodes at 0.05 C rate.

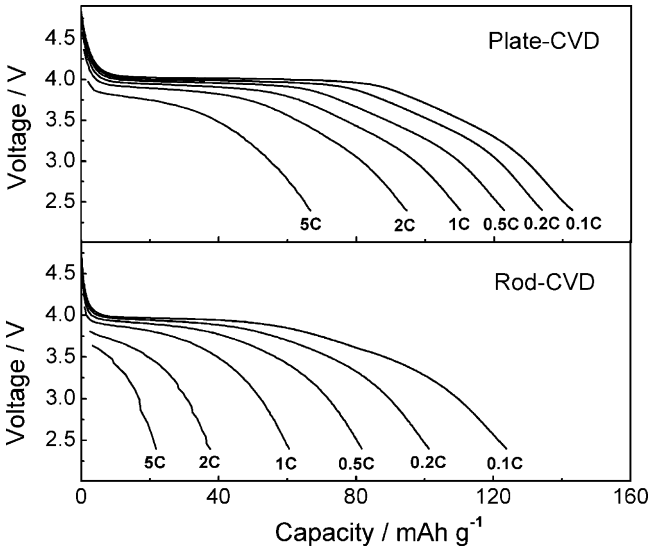

Fig. 7. The discharge curves of the $LiMnPO_4$/C electrodes at various rates.

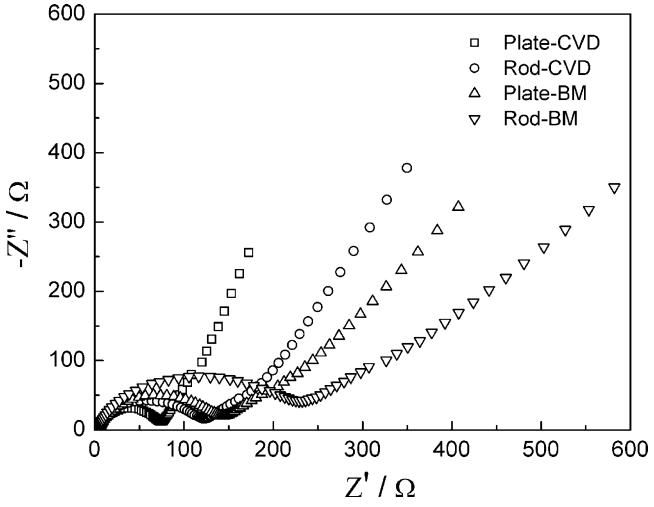

Fig. 8. Nyquist plots the $LiMnPO_4$/C electrodes after 10 cycles.

discharge voltage decreases markedly when the current rates exceed 1 C. This big difference can be mainly attributed to the following two reasons. Firstly, the larger specific surface area of the nanoplates increases the electrochemical reaction zone between electrode and electrolyte and results in faster interfacial charge transfer and lower electrode polarization. Secondly, the lithium ion diffusion depth of ca. 18 nm for nanoplates is much shorter than that of 45–65 nm for nanorods. On the other hand, a thinner carbon layer on the surface of nanoplates also makes the lithium ion diffuse quickly. Therefore, the $LiMnPO_4$/C nanoplates can possess superior high rate capability.

The interfacial property between electrode and electrolyte is further examined by AC impedance measurement. Fig. 8 shows Nyquist plots of the cells using four different $LiMnPO_4$/C electrodes at the fully discharged state after 10 cycles. All the spectra exhibit a similar profile, but the semicircle for Li/$LiMnPO_4$ (Plate-CVD) cell is much smaller than that for others, indicating its remarkably smaller charge-transfer impedance. All the positive effects of the $LiMnPO_4$/C nanoplates can arise from the favorable morphology and perfect carbon coating.

4. Conclusions

In conclusion, $LiMnPO_4$ nanoplates and nanorods were successfully prepared by a solvothermal route in water–benzyl alcohol and water–polyethylene glycol systems, respectively. The CVD method is more suitable than ball milling for creating a uniform and effective carbon layer on the $LiMnPO_4$ to enhance the electronic conductivity and reduce Mn dissolution into the electrolyte. The ideal cluster-like microstructure consisting of numerous nanoplates enlarges interfacial area of electrode/electrolyte and shortens solid-state diffusion length of lithium ions, resulting in a fairly good electrochemical performance.

Acknowledgement

This work was supported by National 973 Program (No. 2007CB209700).

References

[1] G. Wang, H. Liu, J. Liu, S. Qiao, G.M. Lu, P. Munroe, H. Ahn, Adv. Mater. 22 (2010) 4944–4948.
[2] C. Delacourt, P. Poizot, M. Morcrette, J.-M. Tarascon, C. Masquelier, Chem. Mater. 16 (2004) 93–99.
[3] H.H. Li, J. Jin, J.P. Wei, Z. Zhou, J. Yan, Electrochem. Commun. 11 (2009) 95–98.
[4] C.A.J. Fisher, V.M. Hart Prieto, M.S. Islam, Chem. Mater. 20 (2008) 5907–5915.
[5] F. Zhou, M. Cococcioni, K. Kang, G. Ceder, Electrochem. Commun. 6 (2004) 1144–1148.
[6] F. Wang, J. Yang, Y. NuLi, J. Wang, J. Power Sources 196 (2011) 4806–4810.
[7] J. Wolfenstine, J. Allen, J. Power Sources 142 (2005) 389–390.
[8] A.K. Padhi, K.S. Nanjundaswamy, J.B. Goodenough, J. Electrochem. Soc. 144 (1997) 1188–1194.
[9] C. Delacourt, L. Laffont, R. Bouchet, C. Wurm, J.-B. Leriche, M. Morcrette, J.-M. Tarascon, C. Masquelier, J. Electrochem. Soc. 152 (2005) A913–A921.
[10] K. Rissouli, K. Benkhouja, J.R. Ramos-Barrado, C. Julien, Mater. Sci. Eng. B98 (2003) 185–189.
[11] Z. Bakenov, I. Taniguchi, Electrochem. Commun. 12 (2010) 75–78.
[12] D. Choi, D. Wang, I.T. Bae, J. Xiao, Z. Nie, W. Wang, V.V. Viswanathan, Y.J. Lee, J.G. Zhang, G.L. Graff, Z. Yang, J. Liu, Nano Lett. 10 (2010) 2799–2805.
[13] S.M. Oh, S.W. Oh, C.S. Yoon, B. Scrosati, K. Amine, Y.K. Sun, Adv. Funct. Mater. 20 (2010) 3260–3265.
[14] C. Hu, H. Yi, H. Fang, B. Yang, Y. Yao, W. Ma, Y. Dai, Electrochem. Commun. 12 (2010) 1784–1787.
[15] H. Yang, X.L. Wu, M.H. Cao, Y.G. Guo, J. Phys. Chem. C 113 (2009) 3345–3351.
[16] F. Teng, S. Santhanagopalan, A. Asthana, X. Geng, S.-I. Mho, R. Shahbazian-Yassar, D.D. Meng, J. Cryst. Growth 312 (2010) 3493–3502.
[17] A.V. Murugan, T. Muraliganth, P.J. Ferreira, A. Manthiram, Inorg. Chem. 48 (2009) 946–952.
[18] K. Saravanan, J.J. Vittal, M.V. Reddy, B.V.R. Chowdari, P. Balaya, J. Solid State Electrochem. 14 (2010) 1755–1760.
[19] Y. Wang, Y. Yang, Y. Yang, H. Shao, Mater. Res. Bull. 44 (2009) 2139–2142.
[20] Y. Wang, Y. Yang, Y. Yang, H. Shao, Solid State Commun. 150 (2010) 81–85.
[21] D. Wang, H. Buqa, M. Crouzet, G. Deghenghi, T. Drezen, I. Exnar, N.-H. Kwon, J.H. Miners, L. Poletto, M. Grätzel, J. Power Sources 189 (2009) 624–628.
[22] P.R. Kumar, M. Venkateswarlu, M. Misra, A.K. Mohanty, N. Satyanarayana, J. Electrochem. Soc. 158 (2011) A227–A230.
[23] H. Nakano, K. Dokko, S. Koizumi, H. Tannai, K. Kanamura, J. Electrochem. Soc. 155 (2008) A909–A914.
[24] D. Morgan, A. Van der Ven, G. Ceder, Electrochem. Solid-State Lett. 7 (2004) A30–A32.
[25] M.S. Islam, D.J. Driscoll, C.A.J. Fisher, P.R. Slater, Chem. Mater. 17 (2005) 5085–5092.